

Crystallization kinetics of amorphous acetonitrile nanoscale films

Cite as: J. Chem. Phys. **154**, 144703 (2021); <https://doi.org/10.1063/5.0045461>

Submitted: 26 January 2021 . Accepted: 25 March 2021 . Published Online: 12 April 2021

 R. Scott Smith,  M. Tylinski,  Greg A. Kimmel, and  Bruce D. Kay

COLLECTIONS

Paper published as part of the special topic on [Fluids in Nanopores](#)



View Online



Export Citation



CrossMark

ARTICLES YOU MAY BE INTERESTED IN

[Reflections on electron transfer theory](#)

The Journal of Chemical Physics **153**, 210401 (2020); <https://doi.org/10.1063/5.0035434>

[Variational design principles for nonequilibrium colloidal assembly](#)

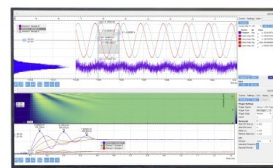
The Journal of Chemical Physics **154**, 014107 (2021); <https://doi.org/10.1063/5.0038652>

[A new one-site coarse-grained model for water: Bottom-up many-body projected water \(BUMPer\). I. General theory and model](#)

The Journal of Chemical Physics **154**, 044104 (2021); <https://doi.org/10.1063/5.0026651>

Challenge us.

What are your needs for
periodic signal detection?



Zurich
Instruments

Crystallization kinetics of amorphous acetonitrile nanoscale films

Cite as: *J. Chem. Phys.* **154**, 144703 (2021); doi: [10.1063/5.0045461](https://doi.org/10.1063/5.0045461)

Submitted: 26 January 2021 • Accepted: 25 March 2021 •

Published Online: 12 April 2021



View Online



Export Citation



CrossMark

R. Scott Smith,^{a)} M. Tylinski, Greg A. Kimmel, and Bruce D. Kay^{a)}

AFFILIATIONS

Physical Sciences Division, Pacific Northwest National Laboratory, Richland, Washington 99352, USA

Note: This paper is part of the JCP Special Topic on Fluids in Nanopores.

^{a)}Authors to whom correspondence should be addressed: Scott.Smith@pnnl.gov and Bruce.Kay@pnnl.gov

ABSTRACT

We measure the isothermal crystallization kinetics of amorphous acetonitrile films using molecular beam dosing and reflection adsorption infrared spectroscopy techniques. Experiments on a graphene covered Pt(111) substrate revealed that the crystallization rate slows dramatically during long time periods and that the overall kinetics cannot be described by a simple application of the Avrami equation. The crystallization kinetics also have a thickness dependence with the thinner films crystallizing much slower than the thicker ones. Additional experiments showed that decane layers at both the substrate and vacuum interfaces can also affect the crystallization rates. A comparison of the crystallization rates for CH₃CN and CD₃CN films showed only an isotope effect of ~1.09. When amorphous films were deposited on a crystalline film, the crystalline layer did not act as a template for the formation of a crystalline growth front. These overall results suggest that the crystallization kinetics are complicated, indicating the possibility of multiple nucleation and growth mechanisms.

Published under license by AIP Publishing. <https://doi.org/10.1063/5.0045461>

I. INTRODUCTION

Acetonitrile is a common laboratory solvent used in a variety of applications. Because it is aprotic and has a large dipole moment (3.92 D), it is widely used in electrochemical and organic synthetic applications where a nonaqueous solvent is required.^{1–9} There is also interest in its existence in comets and planetary systems.^{10–18} The simple hydrocarbons, including nitriles, are believed to play an important role in the formation of more complex organic molecules in the solar system. The characterization and detection of these smaller precursor molecules in the condensed phase at astrophysical temperatures are requisite to understanding the reaction mechanisms of larger species.^{19–22}

In some recent work, we used molecular beam dosing, temperature programmed desorption (TPD), and reflection adsorption infrared spectroscopy (RAIRS) to study the behavior of acetonitrile films deposited at low temperatures (<120 K) on a variety of surfaces.^{23,24} In the first paper, we studied the interactions and the structure of acetonitrile on Pt(111) and graphene surfaces.²³ We found that on Pt(111), the monolayer desorption kinetics were first-order with activation energies ($\sim 75 \pm 4$ kJ/mol) consistent with chemisorption on the substrate. On graphene, the

monolayer desorption kinetics were zero-order, indicating that acetonitrile is physisorbed and has established equilibrium between 2D islands and isolated molecules. These interpretations were supported by RAIRS experiments. When acetonitrile was deposited on Pt(111) at >100 K, the spectra were consistent with the formation of the μ configuration proposed by others, where the CN triple bond is converted to a double bond and the nitrogen and central carbon atoms form single bonds with the neighboring platinum atoms.^{1,25,26} At low deposition temperatures <100 K, the N-top configuration (N end interacting with Pt perpendicular to the surface) was observed, which has also been observed by others.^{2,3,27} On graphene, the RAIRS spectra were consistent with the acetonitrile lying parallel to the surface for monolayer coverages at all deposition temperatures.

In the second paper, we studied the structure of acetonitrile multilayers.²⁴ Crystalline acetonitrile has two polymorphs: a low-temperature (LT) phase that is thermodynamically stable below 217 K and a high temperature (HT) phase that is thermodynamically stable between 217 K and its melting point at 229 K.^{18,28–34} The HT crystal structure consists of anti-parallel dimers with two acetonitrile molecules aligned side-by-side with the methyl end (positive) of one molecule aligned with the CN end (negative) of the second one.

In the LT crystal structure, adjacent acetonitrile molecules interact with their molecular axes perpendicular to each other.^{31,32} Despite the LT polymorph being thermodynamically favored below 217 K, for acetonitrile films vapor deposited at temperatures below 217 K, the higher free energy HT phase is typically observed. The reason is likely due to the differences in the kinetic barriers for crystallization.^{33,34} We observed that the formation of a particular crystalline phase depended on a combination of deposition temperature and the underlying substrate. We were able to obtain the elusive LT phase by growing the films on graphene or crystalline decane at a deposition temperature of 120 K.

In the present paper, we measure the isothermal crystallization kinetics of amorphous acetonitrile films using molecular beam dosing and RAIRS techniques. Experiments are performed on a graphene covered Pt(111) substrate so that the interactions with the Pt(111) surface do not complicate the crystallization kinetics. We present results for a range of film thicknesses, L (50–1000 ML), and isothermal temperatures (105–112 K). We also explored interface effects on the kinetics by using decane layers underneath and on top of the acetonitrile film and crystalline templates. We find that the thickness and interface dependence of the crystallization kinetics cannot be described by a simple crystallization mechanism. These results suggest that the crystallization kinetics are complicated and that there are likely multiple nucleation and growth mechanisms.

II. EXPERIMENTAL

The experiments were conducted in an ultra-high vacuum chamber (base pressure $<10^{-10}$ Torr) equipped with capabilities for molecular beam dosing, temperature programmed desorption, and reflection adsorption infrared spectroscopy (RAIRS), which have been previously described in detail.^{35,36} Films were deposited onto a 1 cm diameter graphene covered Pt(111) single crystal. The graphene layer was grown by heating the Pt(111) to 1100 K and exposing it to an incident beam of decane.³⁷ The integrity of the graphene layer was not affected by the interactions with acetonitrile

as we have observed for other species.^{38,39} This allowed us to perform repeated experiments without cleaning or regrowing the layer. This was not the case for the Pt(111) surface where previous experiments with acetonitrile required frequent sputter and annealing cycles to maintain a clean surface.²³ Thus, with a graphene covered Pt(111) surface, we were able to acquire a much larger dataset than would have been possible on the Pt(111) surface. The sample temperature was controlled using a closed cycle helium cryostat and resistive heating through two tantalum wires spot welded to the backside of the Pt(111). The temperature was measured with a K-type thermocouple to the Pt(111) sample and was calibrated by comparing the multilayer desorption rates of Ar, Kr, and water with their published vapor pressures.^{40–43} We estimate an absolute accuracy of ± 2 K.

The chemicals used in the experiments were anhydrous acetonitrile (Glen Research, 99.8%), deuterated acetonitrile (Cambridge Isotope Laboratories, 99.8%), and decane (Sigma-Aldrich, 99%). The acetonitrile films were deposited at normal incidence with a flux of 1.11 ML/s, where 1 ML was defined as the time needed to saturate of the monolayer desorption feature on the graphene covered Pt(111) surface.²⁴ The film thicknesses, L , were not directly measured. Instead, L is reported here as the coverage in monolayers. Based on the density of acetonitrile, we expect 1 ML to be ~ 0.44 nm. The reflection adsorption infrared spectra (RAIRS) were acquired using a Bruker Vertex 70 FTIR spectrometer with a narrow band MCT detector. The infrared beam was incident on the sample at an angle of $82^\circ \pm 1^\circ$ from normal, and the spectra were acquired with a resolution of 4 cm^{-1} .

III. RESULTS

A. Approach for measuring acetonitrile crystallization

In this section, we present the approaches used to analyze the crystallization kinetics for all the results in this paper. Figure 1 displays a time series of RAIRS spectra obtained from a 200 ML acetonitrile film that was deposited at 60 K and then heated to and held at

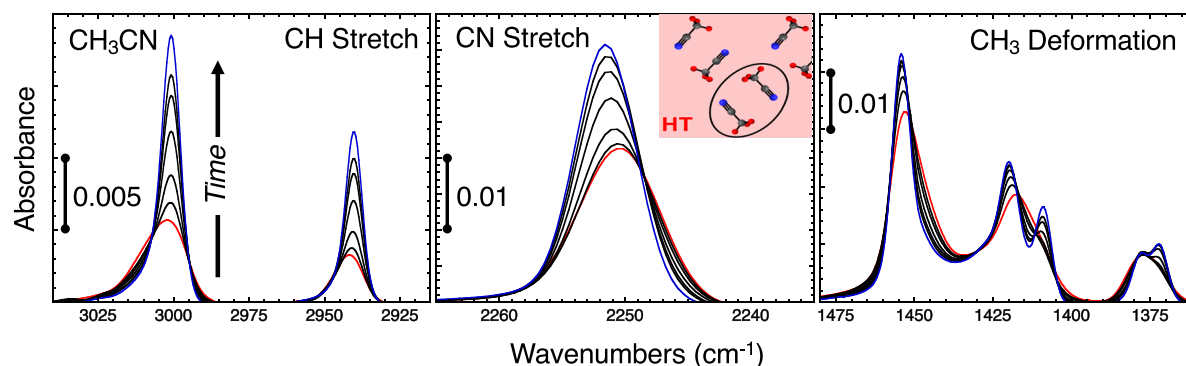


FIG. 1. Time series of RAIRS spectra obtained from a 200 ML thick amorphous acetonitrile film deposited at 60 K and then heated to and held at 108 K. The film was deposited on a graphene covered Pt(111) substrate. The CH_3 stretch ($2915\text{--}3050 \text{ cm}^{-1}$, left panel), the CN stretch ($2235\text{--}2265 \text{ cm}^{-1}$, middle panel), and the CH_3 deformation ($1360\text{--}1480 \text{ cm}^{-1}$, right panel) spectral regions. The initial spectrum (red curve) is acquired at $t = 0$ s of the isothermal time period, and the last one (blue curve) is acquired at $t = \sim 3400$ s. The time evolution of the spectra shows the crystallization to the high temperature (HT) crystalline phase (see the inset in the middle panel).

108 K. Shown are the CH₃ stretch (2915–3050 cm⁻¹), the CN stretch (2235–2265 cm⁻¹), and the CH₃ deformation (1360–1480 cm⁻¹) spectral regions. The peak assignments are consistent with those in the literature.^{18,30,44} The peaks in all three spectral regions exhibit similar behavior, with the peaks in the initial spectrum (red curves) being relatively broad, narrowing in the subsequent spectra, and then evolving to relatively sharp peaks in the final spectrum (blue curves). Also note that the sets of spectra for all the peaks have isosbestic points. Isosbestic points are indicative of a transformation from one state to another; in this case, the transformation from amorphous to crystalline acetonitrile. As described in Sec. I, acetonitrile has two crystalline polymorphs (LT and HT) and the phase that is formed at low temperatures (<130 K) depends on both the substrate and deposition conditions. In the present work, the deposition and annealing conditions resulted in the formation of the metastable HT polymorph.

In Fig. 2, we illustrate the process used to obtain the crystallization kinetics from the RAIRS spectra. Figure 2(a) displays the

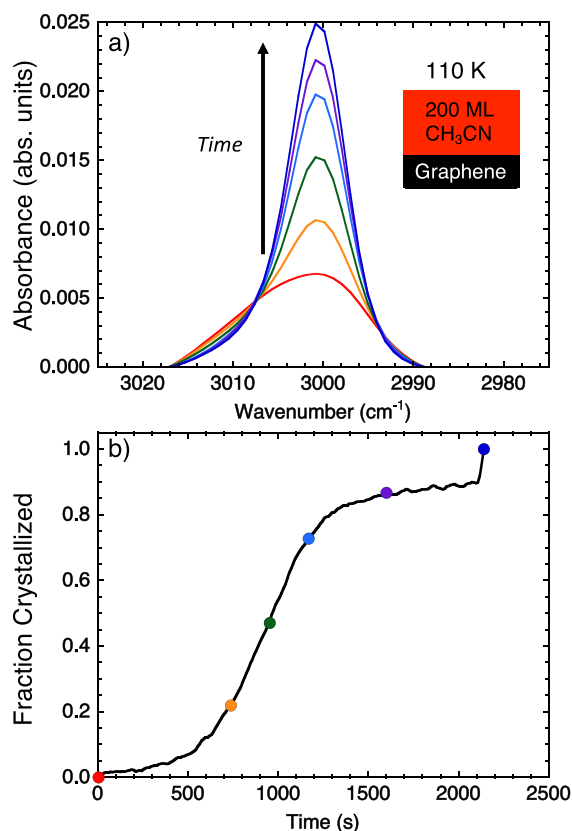


FIG. 2. (a) Time series of RAIRS spectra obtained from a 200 ML thick acetonitrile film deposited on a graphene covered Pt(111) substrate at 60 K and then heated to and held at 110 K. The initial spectrum (red curve) was taken at $t \sim 0$ s. The final spectrum (blue curve) was acquired at the end of the isothermal experiment after heating to 120 K and annealing for 100 s. (b) The fraction crystallized vs time calculated from 200 RAIRS spectra from the acetonitrile film in panel (a). The solid circles are the fraction crystallized values for the color-coded corresponding spectra shown in (a).

asymmetric CH₃ stretch peak for a time series of RAIRS spectra obtained from a 200 ML acetonitrile film held at 110 K. Analysis of all the other peaks gave the same overall results, but the data from the asymmetric CH₃ stretch peak had less statistical noise. For this reason, the CH₃ asymmetric stretch peak was used for all the results presented in this paper. There are several ways to extract the fraction crystallized from the RAIRS spectra, including using the peak height or fitting the intermediate spectra to a linear combination of the 100% amorphous and 100% crystalline spectra. Here, we used the ratio of the integrated area between the two isosbestic points to the area difference between the fully amorphous spectrum ($x = 0$) and the fully crystalline spectrum ($x = 1$) to calculate the fraction crystallized of the intermediate spectra. Figure 2(b) is a plot of the fraction crystallized (black solid line) vs time obtained from the time series of 200 RAIRS spectra from the film shown in Fig. 2(a). The solid circles are the fraction crystallized for the corresponding RAIRS spectra (color coded) in Fig. 2(a). The fraction crystallized increases slowly from 0 to ~ 500 s, followed by a faster increase from 500 to ~ 1400 s, and then returns to a slow increase from 1500 to 2100 s.

Because the fraction crystallized did not reach a point where it stopped increasing, it was not clear if the film had completely crystallized. To check this, at the end of the isothermal experiment, the film was heated to 120 K and annealed for 100 s. When the temperature was then reduced back to 110 K, there were no further changes to the IR spectra. This is the final spectrum (blue curve) in Fig. 2(a). Based on the slope of the slow crystallization region, we estimate that at this temperature, complete crystallization would take at least another 1500–2000 s. Because these additional data do not dramatically change the overall shape of the crystallization curve, we did not extend the isothermal experiments for this additional time. We defined the annealed spectrum obtained after the isothermal experiment as being that for a completely crystalline film. The integrated area of this spectrum was used to define the area for a completely crystallized film to calculate the fraction crystallized [see the blue solid circle in Fig. 2(b)]. We used this method for all the experimental results in this paper.

The sigmoidal-like line shape in Fig. 2(b) is commonly observed for kinetic processes in solids and can often be fit by the Avrami equation,^{45,46}

$$x(t) = 1 - e^{-(kt)^n}, \quad (1)$$

where x is the fraction crystallized, k is a phenomenological rate constant, and n is related to the crystallization mechanism. For example, a mechanism where there is random nucleation and isotropic three-dimensional growth would yield a value of $n = 4$. In the subsequent analysis, we define τ as the time when the fraction crystallized is equal to 0.632, i.e., when $x(t) = 1 - e^{-1}$. This is equivalent to τ being defined as $1/k$ in Eq. (1). However, in Fig. 2(b), the continued slow increase in the fraction crystallized curve at long times cannot be fit well by the Avrami equation, which plateaus to a flat line at a long time. The inability of the Avrami equation [Eq. (1)] to fit the fraction crystallized vs time curves is unrelated to the definition of the endpoint (the post experiment annealing). In fact, no single combination of k and n in Eq. (1) can accurately describe both τ and the continued slow increase in the fraction crystallized at long times. As shown below, the kinetics for the crystallization of acetonitrile films likely requires multiple mechanisms.

Another factor that can affect the crystallization kinetics is the temperature of the substrate during deposition of the amorphous film. Figure 3 displays the fraction crystallized vs time curves for 200 ML films held at 108 K. The films were deposited on a graphene covered Pt(111) substrate at various deposition temperatures from 30 to 75 K. The results for films deposited from 30 to 60 K are displayed in Fig. 3(a). The curves shift to longer times, which means that the crystallization rate decreases with the increase in the deposition temperature. The results for films deposited from 60 to 75 K displayed in Fig. 3(b) show that the curves shift to shorter times, meaning that in this temperature range, the crystallization rate increases with the increase in the deposition temperature. The inset in Fig. 3(b) is a plot of the τ vs deposition temperature for all the crystallization experiments in Fig. 3.

The results show that there is a peak in the value of τ at deposition temperatures between 55 and 60 K. The increase in τ (decrease in the crystallization rate) from 30 to 60 K can be explained by the porosity of the acetonitrile films. In a prior work, we showed that acetonitrile films are porous when deposited at temperatures below 50 K, even when dosed at normal incidence.²⁴ The increased porosity means more surface area and the possibility of more facile nucleation

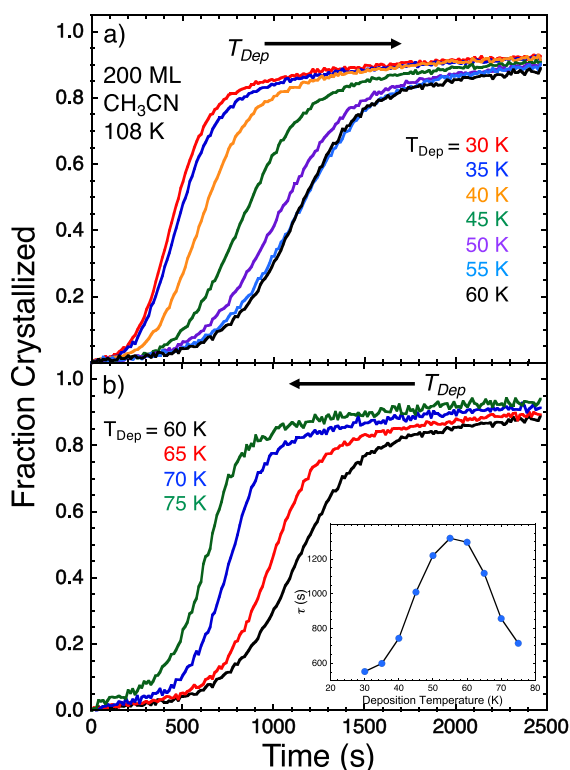


FIG. 3. The fraction crystallized vs time curves for a 200 ML acetonitrile film at 110 K. The film was deposited on a graphene covered Pt(111) substrate at various deposition temperatures. (a) Fraction crystallized vs time curves for film deposition temperatures of 30 (red), 35 (blue), 40 (orange), 45 (green), 50 (purple), 55 (light blue), and 60 K (black). (b) Fraction crystallized vs time curves for film deposition temperatures of 60 (black), 65 (red), 70 (purple), and 75 K (light blue). The inset in (b) shows the non-monotonic behavior of τ on growth temperature.

because molecules on the surface are less constrained than those in the bulk. This has been observed in the crystallization kinetics of amorphous solid water (ASW) films.^{47–49} The decrease in τ (increase in the crystallization rate) above ~ 60 K could be due to the formation of pre-nuclei during deposition and this has been observed in ASW film crystallization.³⁵ Another possible explanation is that the deposition temperature affects the structure of the amorphous deposited film, creating more stable amorphs or stable glasses.^{50–53} These more “stable” glasses could take longer to crystallize. Regardless of the reason for the observations, for consistency, in the rest of this paper, all the acetonitrile films were prepared at a deposition temperature of 60 K.

B. Crystallization kinetics of acetonitrile films on graphene

In this section, we study the crystallization kinetics of acetonitrile films for a range of film thicknesses and isothermal temperatures. The experiments were conducted on a graphene covered Pt(111) substrate to prevent the covalent interactions of acetonitrile that occur on bare Pt(111), which could complicate the crystallization kinetics.^{23,26,54} Isothermal experiments were conducted in 1 K increments from 105 to 112 K and for film thicknesses of 50, 100, 200, 400, 600, 800, and 1000 ML. Figure 4 displays the results at 112 K [Fig. 4(a)], 109 K [Fig. 4(b)], and 106 K [Fig. 4(c)]. As expected, the crystallization rates increase, i.e., the sets of crystallization curves shift to earlier time, with the increase in temperature. At a given temperature, the crystallization curves shift to shorter times with the increase in thickness, meaning that the crystallization rate increases with the film thickness.

Figure 5 displays the τ values for the experiments in Fig. 4 and data from other isothermal temperature experiments not shown there. A plot of τ vs film thickness for each isothermal temperature is shown in Fig. 5(a). The plot shows that τ monotonically decreases with the increase in the film thickness for all temperatures, although the thickness dependence is stronger at lower temperatures. For example, at 105 K (black solid circles), τ for the 50 ML film is ~ 11 times longer than that for the 1000 ML film, whereas at 112 K (red solid circles), the same comparison is only a factor of ~ 2.1 .

The results shown in Fig. 5(a) are not consistent with a simple picture of homogeneous (i.e., bulk) nucleation and isotropic growth. To understand why, we first note that for these experiments, a large number of crystalline nuclei form and the resulting films are polycrystalline.⁵⁵ In that case, the typical grain size in the film, X_{gr} , relative to the film thickness, L , is an important property of the films that affects the kinetics.^{56,57} The typical grain size is given by $X_{gr} = (G/J_b)^{1/4}$, where G is the crystalline growth rate and J_b is the bulk nucleation rate. For bulk nucleation and growth and $X_{gr} \gg L$, τ would be proportional to $L^{-1/3}$, while τ would be independent of L for $X_{gr} \ll L$.⁵⁶ Specifically, if $X_{gr} \gg L$, then the growth would be approximately two dimensional (i.e., the grains would look like thin disks) and the exponent, n , in the Avrami equation [Eq. (1)] would be ~ 3 . In that case, $\tau = (J_A G^2)^{-1/3}$, where J_A is the nucleation rate per unit area (i.e., the areal nucleation rate). If J_b is independent of L , then $J_A = J_b L$ and $\tau = (J_b L G^2)^{-1/3} \sim L^{-1/3}$.⁵⁶ In contrast, $X_{gr} \ll L$ corresponds to the bulk limit where $n = 4$ and $\tau = (J_b G^3)^{-1/4} \sim L^0$. For an experiment that spanned thicknesses from $L \ll X_{gr}$ to $L \gg X_{gr}$, a log-log plot of τ vs L would have a slope of $-1/3$ for small L

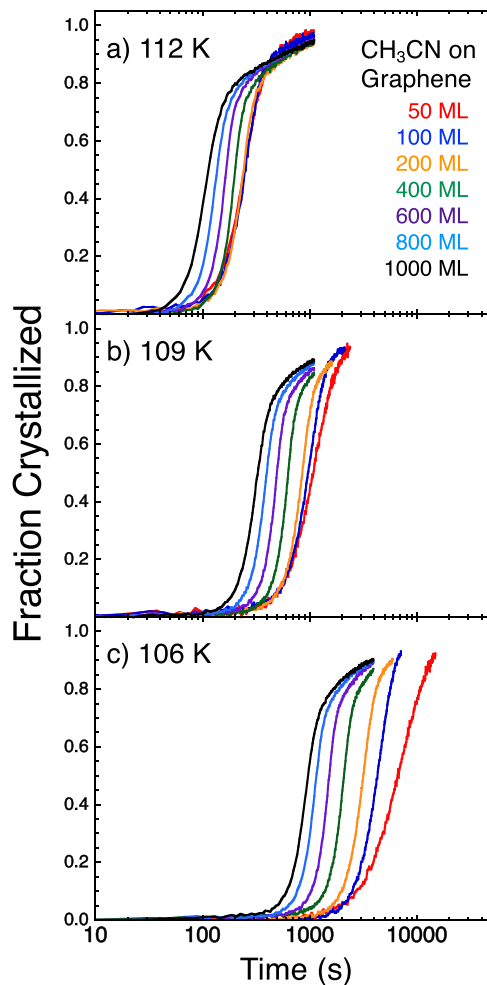


FIG. 4. Fraction crystallized vs time curves for acetonitrile films deposited on a graphene covered Pt(111) substrate at a deposition temperature of 60 K. The film thicknesses are 50 (red curves), 100 (blue curves), 200 (orange curves), 400 (green curves), 600 (purple curves), 800 (light blue curves), and 1000 ML (black curves). (a) Fraction crystallized curves for films heated to 112 K. (b) Fraction crystallized curves for films heated to 109 K. (c) Fraction crystallized curves for films heated to 106 K.

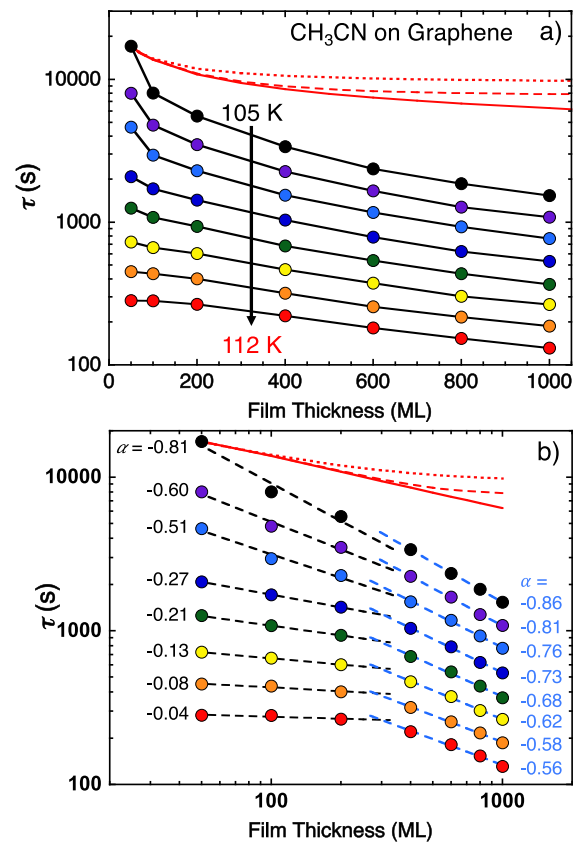


FIG. 5. (a) Plot of τ values from acetonitrile crystallization experiments for film thicknesses from 50 to 1000 ML at various temperatures. The experiments were conducted at temperatures of 105 (black circles), 106 (purple circles), 107 (light blue circles), 108 (blue circles), 109 (green circles), 110 (yellow circles), 111 (orange circles), and 112 K (red circles). The red lines show example τ vs L curves where G and J_b were chosen to match τ for a 50 ML film at 105 K and have $X_{gr} = 400$ (dotted line) and 600 ML (dashed line). The red solid line indicates a τ dependence of $L^{-1/3}$. (b) A log-log plot of the τ values in (a). Also plotted are power law fits, $\tau \sim L^\alpha$, to the 50–200 ML data (black dashed lines) and the 400–1000 ML data (blue dashed lines) and the corresponding fit values for α .

that smoothly increased to 0 for large L .⁵⁷ The red lines in Fig. 5(a) show example τ vs L curves where G and J_b were chosen to match τ for a 50 ML film at 105 K and have $X_{gr} = 400$ (dotted line) and 600 ML (dashed line). The red solid line is for a τ dependence of $L^{-1/3}$.

Figure 5(b) shows a log-log plot of the data from Fig. 5(a). Except for $T = 105$ K, the data show significant deviations from any simple power law. An important observation is that the steepness on all the curves increases with the increase in coverage. This is opposite to the behavior expected for homogeneous nucleation and growth that was discussed above [see the red lines in Fig. 5(b)]. Furthermore, the films appear to display a different behavior for thicknesses larger or smaller than ~ 300 ML. Figure 5(b) shows power law fits, $\tau \sim L^\alpha$, for the 50–200 ML data (black lines) and the 400–1000 ML data (blue lines) and the corresponding values for α . Note

that for $L \geq 400$ ML, α is always significantly less than $-1/3$, rather than asymptotically approaching zero as one would expect for bulk nucleation. Note that in some experiments where the sample quickly crystallizes after a single crystalline nucleus forms, the crystallization time scales as V^{-1} , where V is the volume of the sample. Defining the crystallization time in such situations has been discussed previously.⁵⁸ However, since numerous crystalline nuclei form during our experiments, this explanation is not applicable here.^{56,57} As discussed in more detail below, these and other results suggest that the crystallization of the acetonitrile films is a combination of multiple nucleation and growth mechanisms.

Arrhenius plots of the τ data in Fig. 5 are shown in Fig. 6(a). The solid lines are fits to the τ values for films of the same thickness. The slopes for films with thicknesses from 400 to 1000 ML are nearly parallel, but below 400 ML, the slopes increase with the decrease in

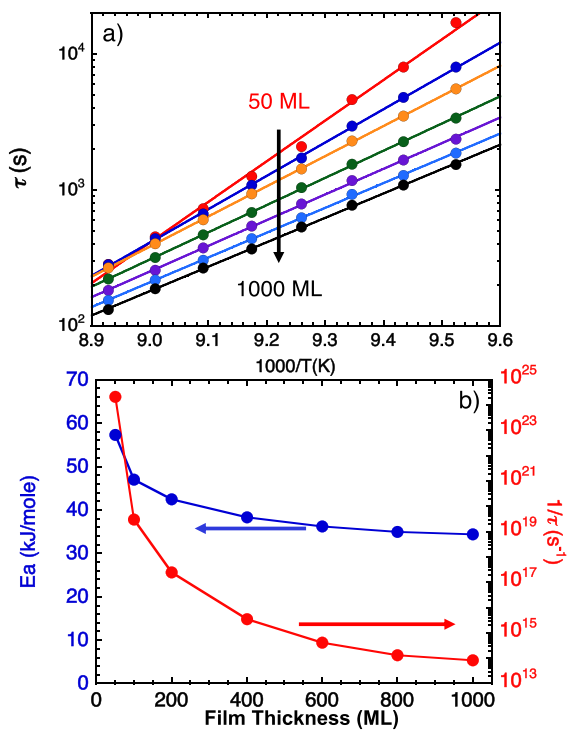


FIG. 6. (a) Arrhenius plot of the τ values in Fig. 5 for various film thicknesses. The experiments were conducted at film thicknesses of 50 (red circles), 100 (blue circles), 200 (orange circles), 400 (purple circles), 600 (purple circles), 800 (light blue circles), and 1000 ML (black circles). The lines are Arrhenius fits to the data points. (b) Plot of the Arrhenius parameters obtained from the fits displayed in (a). The scale of the activation energies (blue circles) is on the left-hand side and the scale of the prefactors (red circles) is on the right-hand side.

film thickness. The extracted Arrhenius fit parameters are displayed in Fig. 6(b). For film thicknesses from 1000 to 400 ML, the activation energies (blue solid circles), E_a , vary over a narrow range from ~ 34 to 39 kJ/mol. For film thicknesses below 400 ML, the E_a increases steeply to near 60 kJ/mol for the 50 ML film. A similar trend is observed for the prefactors, $\nu = 1/\tau_0$ (red solid circles), with the values for film thicknesses from 1000 to 400 ML being relatively close, ranging from 1×10^{14} to $5 \times 10^{15} \text{ s}^{-1}$, and the prefactors for film thicknesses below 400 ML increasing to a value of $2 \times 10^{24} \text{ s}^{-1}$. The prefactors for the thinner films are larger than the typically observed range of 10^{13} – 10^{17} s^{-1} and suggest that there are multiple crystallization mechanisms or that the kinetics are dependent on the film thickness. If this is the case, a simple interpretation of the Arrhenius parameters is not possible.

As discussed above [Eq. (1)], the value of n obtained from fits to the Avrami equation is often used to gain insight into the crystallization mechanism. However, obtaining good fits to the crystallization curves in Fig. 4 is difficult because of the slow crystallization at longer time. Another approach is to rearrange Eq. (1) to the following form:

$$\ln \left[\ln \left(\frac{1}{1-x} \right) \right] = n \ln \left(\frac{t}{\tau} \right). \quad (2)$$

Using Eq. (2), an estimate of n can be obtained from a plot of the left-hand side of Eq. (2) vs $\ln(t/\tau)$. The procedure is illustrated in Fig. 7 for the 108 K crystallization curves where the solid lines are calculated from the experimental data for all film thicknesses. For reference, the dashed lines are calculated using the assumed fixed values for n . The curves for most film thicknesses initially have n values between 3 and 4, with the 50 ML film having an n between 2 and 3. Above the $t = \tau$ point, the n values, for all of the films, change to a value closer to 0.5. Clearly, there is not a single value of n that can describe the overall crystallization mechanism for a given isothermal experiment. Furthermore, the plot shows that there is no single mechanism that can describe the crystallization kinetics for all the different film thicknesses.

The results presented in this section show that the crystallization kinetics of acetonitrile films do not follow a simple mechanism. Both the thickness dependence and the slow crystallization rates at long times suggest that the kinetics are complicated and could involve a combination of bulk and interfacial nucleation and growth processes. In Sec. III C, we explore the effects of various interfaces on the crystallization kinetics.

C. Interface effects on the crystallization kinetics of acetonitrile films

In this section, we study the effects of various interfaces on the acetonitrile crystallization kinetics. In prior work on the crystallization of ASW films, the films were deposited on top of a decane layer to eliminate possible substrate-induced nucleation that might occur on the ordered graphene.^{47–49} The idea is that amorphous decane deposited at a low temperature will not form an ordered surface, thus minimizing the possibility of it acting as a nucleation or growth template.

Figure 8 displays the crystallization results for 100 ML films of acetonitrile deposited on various thicknesses of decane at 109 K. The results in Fig. 8(a) show that the fraction crystallized curves shift

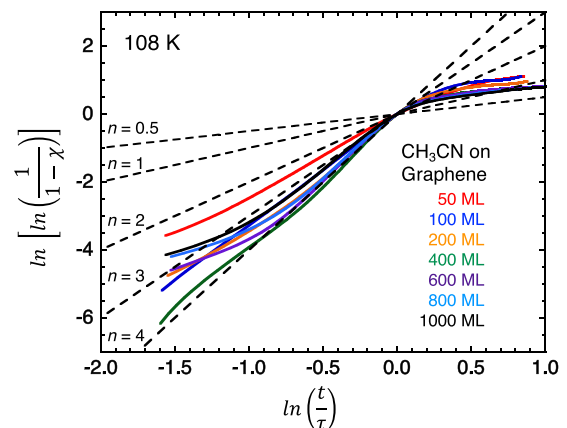


FIG. 7. Analysis of the fraction crystallized curves for various acetonitrile film thicknesses on a graphene covered Pt(111) substrate at 108 K. The film thicknesses are 50 (red solid line), 100 (blue solid line), 200 (orange solid line), 400 (green solid line), 600 (purple solid line), 800 (light blue solid line), and 1000 ML (black solid line). The dashed lines are calculated using Eq. (2) for various assumed values for n of 0.5, 1, 2, 3, and 4.

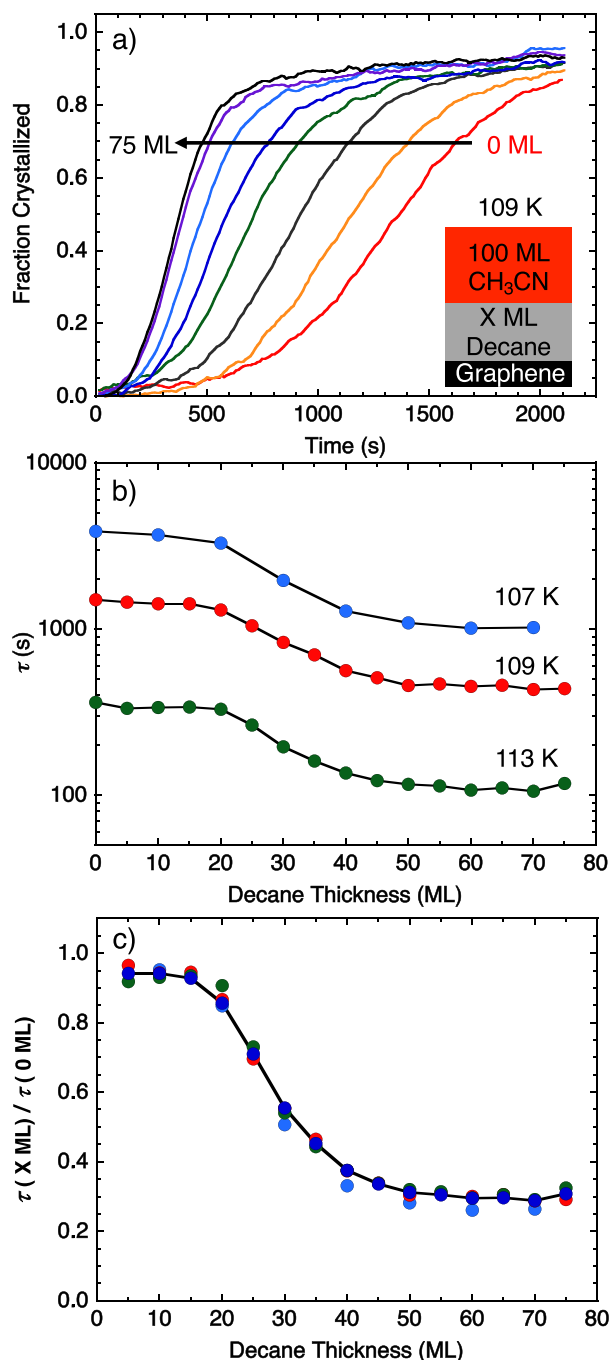


FIG. 8. (a) Fraction crystallized vs time curves for 100 ML thick acetonitrile films at 109 K deposited onto various underlayer thicknesses of decane. The decane underlayer thicknesses displayed are 0 (red curve), 20 (orange curve), 25 (dark gray curve), 30 (green curve), 35 (blue curve), 40 (light blue curve), 55 (purple curve), and 75 ML (black curve). (b) Plot τ values vs decane underlayer thicknesses for crystallization experiments at temperatures of 107 (blue circles), 109 (red circles), and 113 K (green circles). (c) Plot of the τ values vs decane layer thickness shown in (b) rescaled by their respective τ values with no decane underlayer (0 ML data). The solid line is a fit to the combined rescaled τ values and is intended only to show the data trend.

to earlier time with the increase in the decane layer thickness. The τ values from these experiments and those obtained at other temperatures are plotted in Fig. 8(b). The results for all temperatures show a similar trend, with τ being relatively constant for decane layers less than 20 ML, decreasing between 20 and 50 ML, and then being relatively constant above 50 ML. The relative magnitude of the thickness dependence is the same for all temperatures, which is demonstrated in Fig. 8(c) by rescaling τ by the value obtained with no decane underlayer (0 ML point). The rescaling collapses all the τ values into a single curve. The crystallization kinetics dependence on the thickness of the decane layer suggests that the kinetics are affected by being further from the Pt(111) substrate or that a minimum decane film thickness is needed to achieve a consistent surface structure. Because the effect saturates above ~ 50 ML, in subsequent experiments with decane underlayers, we will use a 70 ML thick layer.

Figure 9 shows the results for acetonitrile films grown in four different configurations and crystallized at 110 K. Plotted are the τ values vs acetonitrile film thickness for films grown directly on graphene (black diamonds), on a 70 ML decane underlayer (red squares), on graphene with a 70 ML decane overlayer (blue triangles), and on a 70 ML decane underlayer and capped with a 70 ML decane overlayer (green circles). Clearly, the presence of a decane underlayer, a decane overlayer, or both has an effect on the crystallization kinetics. The decane underlayer and overlayer appear to affect the kinetics differently. For example, the crystallization rates at most thicknesses are faster for the two configurations with a decane underlayer (red squares and green circles) than for the two configurations without an underlayer (black diamonds and blue triangles). This result suggests that the graphene substrate does not act as a nucleation/growth template or at least not as the primary nucleation mechanism.

The decane overlayer also has an effect on the crystallization kinetics although the effect is less pronounced for thicker films. For

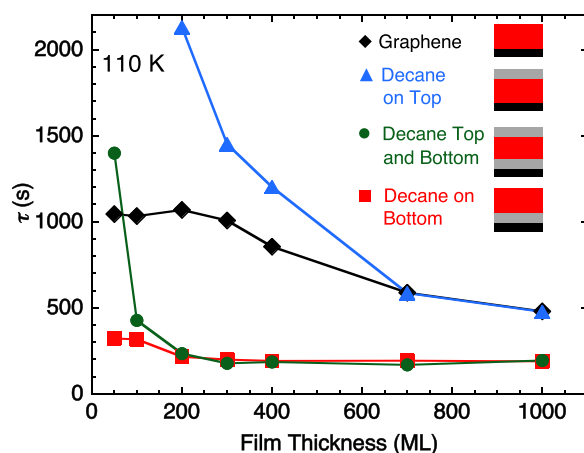


FIG. 9. Plot of τ values vs film thickness for acetonitrile films crystallized at 110 K in four different film configurations. The results are for films grown directly on graphene (black diamonds), on a 70 ML decane underlayer (red squares), on graphene with a 70 ML decane overlayer (blue triangles), and on a 70 ML decane underlayer and capped with a 70 ML decane overlayer (green circles).

example, comparing the two configurations with decane underlayers (red squares and green circles), the τ values are nearly the same at all thicknesses except for the 50 ML film where τ increases dramatically for the configuration that also has a decane layer on top (green circles). A similar trend is observed for the two configurations without decane underlayers (black diamonds and blue triangles). In this case, the τ values are within $\sim 30\%$ for films with thicknesses from 1000 to 400 ML but increase more steeply for thinner films (<300 ML) for the configuration with a decane overlayer. These results suggest that capping the film at the vacuum interface may impede the nucleation at that surface; however, this nucleation source only affects the overall crystallization kinetics for relatively thin films. This suggests that other nucleation mechanisms dominate the crystallization kinetics for thicker films.

Additional experiments were conducted to gain insight into the acetonitrile crystallization kinetic mechanisms. Figure 10 displays the results comparing the crystallization kinetics between the CH_3CN and CD_3CN isotopes. The crystallization curves for 200 ML

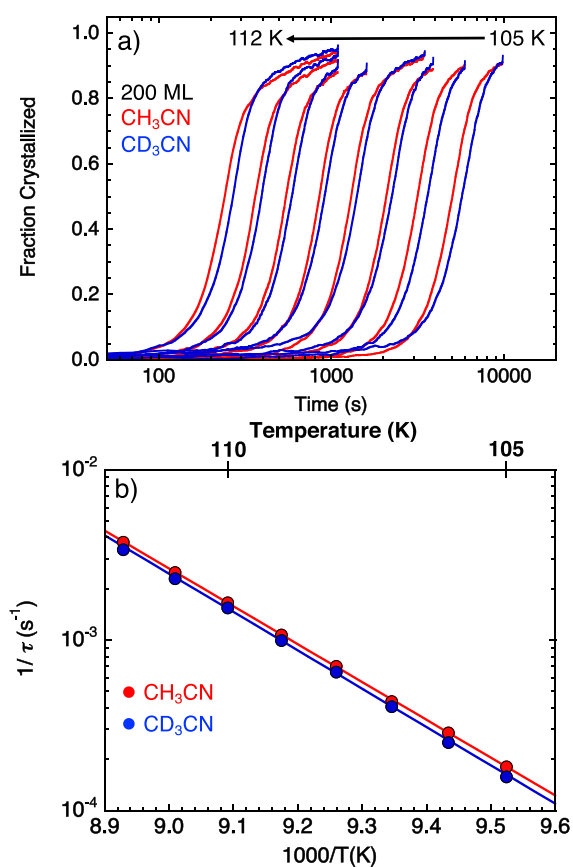


FIG. 10. (a) The fraction crystallized vs time curves for a 100 ML CH_3CN (red curves) and CD_3CN (blue curves) films deposited on a graphene covered Pt(111) for temperatures from 105 to 112 K. (b) An Arrhenius plot of the $1/\tau$ values for the curves displayed in (a). The solid lines are fits that yielded a prefactor of $2.5 \times 10^{17 \pm 2} \text{ s}^{-1}$ and an activation energy of $42.5 \pm 4 \text{ kJ/mol}$ for CH_3CN (red line) and a prefactor of $4.2 \times 10^{17 \pm 2} \text{ s}^{-1}$ and activation energy of $43.0 \pm 4 \text{ kJ/mol}$ for CD_3CN (blue line).

films deposited at 60 K on a graphene covered Pt(111) substrate for a series of isothermal temperatures are displayed in Fig. 10(a). The results show that for all temperatures from 105 to 112 K, the crystallization of CH_3CN (red curves) occurs slightly before CD_3CN (blue curves). An Arrhenius plot of the $1/\tau$ values for the curves is displayed in Fig. 10(b). The solid lines are fits that yielded a prefactor of $2.5 \times 10^{17 \pm 2} \text{ s}^{-1}$ and an activation energy of $42.5 \pm 4 \text{ kJ/mol}$ for CH_3CN and a prefactor of $4.2 \times 10^{17 \pm 2} \text{ s}^{-1}$ and an activation energy of $43.0 \pm 4 \text{ kJ/mol}$ for CD_3CN . The isotope effect is relatively small with the crystallization rate for CH_3CN being only a factor of ~ 1.09 times faster than the deuterated form.

Another factor investigated was the effect that a crystalline template has on the crystallization kinetics. In these experiments, the acetonitrile films were deposited on a 100 ML crystalline layer and capped with 70 ML of decane. The deuterated isotope was used for the crystalline layer so that the CD_3 stretching peaks did not interfere with those for CH_3CN . The films were capped to minimize the possibility of a crystalline growth front forming at the vacuum interface. The fraction crystallized vs time curves for 100 (red curve) and 200 ML (blue curve) thick acetonitrile films at 110 K are shown in Fig. 11(a). The same data are plotted as the number of monolayers crystallized vs time in Fig. 11(b). The slower crystallization rate

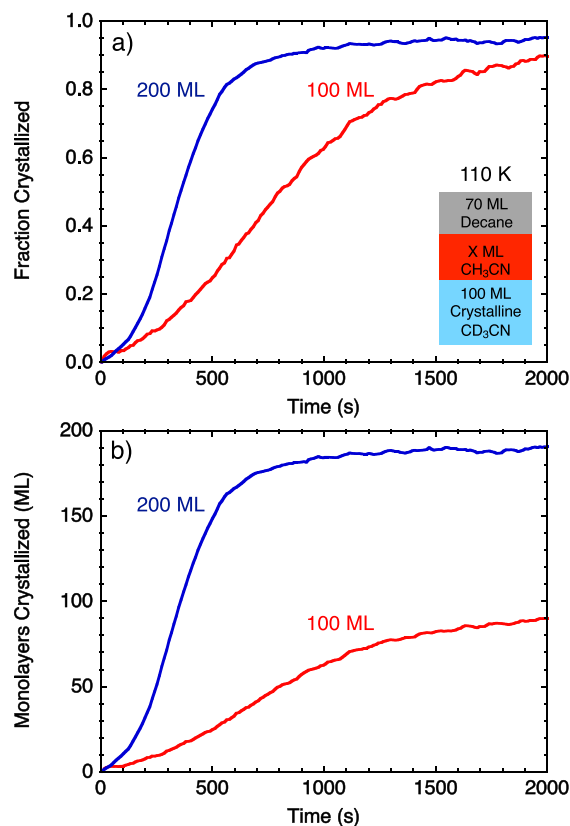


FIG. 11. (a) Fraction crystallized vs time curves for 100 ML (red curve) and 200 ML (blue curve) CH_3CN films at 110 K that were deposited on a 100 ML crystalline CD_3CN layer and then capped with 70 mL of decane. (b) The results from panel (a) plotted as the number of monolayers crystallized vs time.

for the thinner film and the $x(t)$ line shapes in Fig. 11(a) are similar to the observations for non-templated films presented above. One would expect that the presence of a crystalline template would facilitate the formation of a growth front that would dominate the overall crystallization kinetics.⁴⁹ In this scenario, the crystallization front would move through the two films at the same rate, and thus, the thinner film would crystallize sooner. *In addition, the curves showing the number of monolayers crystallized vs time should initially align onto a single straight line with a saturation time that increases the film thickness.* It is clear that the curves [Fig. 11(b)] for the 100- and 200-ML films do not align (or for very long) and that the curves are not linear. This suggests that crystalline growth is not significantly influenced by the crystalline template.

IV. DISCUSSION

The results presented in this paper clearly show that the crystallization kinetics for acetonitrile are complicated. This is demonstrated by the results for films deposited on a graphene layer presented in Figs. 2–7. The first puzzling result is the line shape of the fraction crystallized vs time curves in Figs. 2–4. The curves do not plateau but instead continue to increase at longer times. The continued slow growth at long times has been observed in the growth of nanocrystals and has been attributed to Ostwald ripening.⁵⁹ We do not believe that Ostwald ripening is the explanation here. The reason is that the peak positions and isosbestic points for the spectra in both the fast and slow crystallization rate regions do not change [see Fig. 2(a)]. Prior work on water film crystallization has shown that Ostwald ripening results in changes in the infrared peak shape and position.^{60,61}

Instead, we think that the crystallization mechanism may change when the fraction crystallized approaches one. Support for this interpretation comes from the results in Fig. 7. The plots show that for all film thicknesses, the Avrami n value changes from between 3 and 4 to closer to 0.5–1 when the fraction crystallized is greater than ~ 0.632 (i.e., $1 - e^{-1}$). One explanation could be that there are regions where molecules are trapped and cannot easily convert to the crystalline phase. The two acetonitrile crystalline phases require either parallel (HT) or perpendicular (LT) dimer pairs with their positive (methyl) and negative (CN) ends arranged to maximize their electrostatic interactions. Molecules that are out of alignment may find large activation barriers for realignment once these dimer pairs are formed. Prior work suggests that the amorphous acetonitrile film may consist of randomly oriented (antiparallel dipole-bound) dimer pairs and that large activation barriers may exist to reorient the individual monomers.^{33,34}

The second puzzling result is the thickness dependence of the crystallization kinetics. The data in Fig. 5 show that the crystallization time is a factor of ~ 11 longer for a 50 ML film than for a 1000 ML at 105 K and a factor of ~ 2.1 longer for the same film thicknesses at 112 K. If the crystallization mechanism was dominated by interfacial nucleation, then one would expect the crystallization time to increase with the film thickness as the crystallization growth front moves through a thicker film, but this is not observed. The observed decrease in crystallization times with thickness suggests that bulk nucleation plays a role, while the continued decrease in τ for thick films indicates that the bulk limit has not yet been reached even

for 1000 ML thick films (see Fig. 5). However, several observations are incompatible with a simple model of homogeneous nucleation and growth as follows: (1) The rate of change in the crystallization time vs thickness has the wrong shape [see Fig. 5(b)]. (2) For $T < 109$ K, the ratios of the maximum to minimum nucleation times vs coverage (at a given temperature) are too large [i.e., the ratios are $>(1000/50)^{1/3} \approx 2.71$]. (3) The crystallization prefactors and activation energies depend on the thickness of the films [see Fig. 6(b)], instead of being independent of the thickness. This leads to smaller changes in τ vs thickness at high temperatures compared to lower temperatures (see Fig. 5). (4) Finally, the crystallization kinetics are dependent on the nature of the two interfaces (substrate and vacuum). For example, even for thick films, the nature of the interface changes the crystallization rate by a factor of 2.5 (see the 1000 ML film data in Fig. 9). One would expect the interface effects to be minimal if the mechanism was dominated by bulk nucleation especially in thicker films. Interface effects are known to play a role in crystallization in many systems, including amorphous water films.^{62,63} However, as discussed above, there are many differences in the crystallization kinetics of amorphous water and acetonitrile.^{47–49}

The data suggest that nucleation occurs throughout the films but with a rate that depends on the distance from the interfaces, possibly including nucleation directly at the interfaces. For example, bulk nucleation where the probability increases with the film thickness should be able to reproduce some of the results shown in Fig. 5. Support for a thickness-dependent nucleation rate comes from the Arrhenius parameters shown in Fig. 6. Those data show that the prefactors and activation energies for films thicker than 400 ML have nearly the same values. For films less than 400 ML, the Arrhenius parameters increase with a decrease in thickness, suggesting a change in the crystallization mechanism.

These ideas were explored in Figs. 8 and 9 where decane layers were added to the substrate and vacuum interfaces. The results in Fig. 8 showed that for a given film thickness (100 ML in this case), the crystallization time depended on the thickness of a decane underlayer. This result also seems to contradict the idea that the acetonitrile crystallization is dominated by bulk nucleation. For example, if bulk nucleation was the primary mechanism, then one would expect that for a given film thickness, the crystallization kinetics would be completely independent of the decane layer thickness. Instead of preventing interaction with the graphene surface, the role of the underlayer seems to be to increase the distance of the acetonitrile film from the graphene covered Pt(111) substrate.

The results in Fig. 9 show that the presence of a decane underlayer does affect the crystallization rates. For example, compare the rates of the films with decane underlayers (red squares and green circles) vs those without them (black diamonds and blue triangles). However, it is not clear whether these observations are due to a change in the interface (graphene vs decane) or to the film being further from the surface. There is also an effect of having a decane layer at the vacuum interface. If one compares the two experiments with decane underlayers, the 50 and 100 ML films with a decane cap (green circles) have longer crystallization than those without them (red squares). For films without decane underlayers, comparing films without a decane cap (black diamonds) and those with a decane cap (blue triangles) shows that the effect is even larger.

The observation that a decane cap layer can slow the crystallization rate has been seen previously for the crystallization of amorphous solid water films.^{47–49} The explanation is that molecules at the vacuum interface have more mobility than those in the bulk and that the presence of a decane cap impedes nucleation at the free vacuum interface. Note that for thicker films, the decane cap effect does not affect the crystallization rate, indicating that other nucleation mechanisms are involved.

Experiments comparing the crystallization rates of the CH_3CN and CD_3CN in Fig. 10 showed a weak isotope effect of $k_H/k_D = \sim 1.09$. This is in contrast to the isotope effect for amorphous solid water where the crystallization of H_2O films is a factor of 6.6 times faster than that for D_2O .⁶⁴ Figure 11 shows that the presence of a crystalline template does not result in the formation of a crystalline growth front. The crystallization mechanism for many substances consists of an initial nucleation step that is followed by growth. Typically, the kinetic barrier for nucleation is larger than that for growth, which results in the canonical sigmoidal $x(t)$ line shape (slow, fast, and slow kinetics).^{45,46} The initial slow region is ascribed to an induction period due to the relatively slow nucleation kinetics. The presence of a crystalline template should have eliminated the need for nucleation, resulting in the immediate onset ($\sim t = 0$) of crystallization across the template creating a growth front that moves linearly through the film. The results in Fig. 11 clearly show that this is not the case. This is in contrast to the crystallization of amorphous water films where a crystalline template was used to decouple nucleation and growth, which allowed for the direct and independent measurement of the growth kinetics.⁴⁹ The observations here suggest that the acetonitrile crystallization mechanism is considerably more complicated than that for amorphous solid water.

Clearly, the crystallization of the acetonitrile films involves a combination of multiple nucleation and growth mechanisms. We spent a considerable amount of time and effort in developing kinetic models that included nucleation and growth at the substrate interface, vacuum interface, and in the bulk. The model required prefactors and activation energies for nucleation and growth for each location. We had hoped to directly measure the growth parameters by depositing amorphous films on crystalline templates. However, as shown in Fig. 11, the presence of the crystalline layer did not lead to the formation of a linear crystalline growth front. Furthermore, the data in Fig. 8 suggest that the distance from the graphene covered Pt surface is an additional factor in the kinetics. Specifically, being closer to the surface acts to retard the crystallization. We incorporated the idea of a “dead zone,” a region near the surface where the kinetics were slowed, into some preliminary kinetic models. This improved the results; however, with so many undetermined parameters in the model, assigning in physical significance to the results is difficult. We are currently still working on sorting out the kinetics for this complicated system.

V. SUMMARY

The combined results in this paper show that the crystallization kinetics for nanoscale acetonitrile films are very complicated. It is likely that this complexity is due to the relatively large dipole moment (3.92 D) of acetonitrile. It is possible that the crystallization kinetics could be affected by the electric field that extends from

the graphene covered Pt(111) metal substrate. In this scenario, the highly polar acetonitrile molecules would align or partially align due to the field arising from image potentials, and this could make molecular rearrangements more difficult due to a higher energy barrier. If this is the case, it could explain the slow crystallization kinetics of thin films and why the crystallization rate increases for films with a decane underlayer. The idea is that the decane layer moves the acetonitrile film to a distance where it is not affected by the surface electric fields. However, the idea that the distance from the substrate affects the crystallization kinetics is conjecture and further experiments are needed to test this idea. In future work, we will work on understanding the crystallization kinetics using numerical simulations that treat both bulk and interface nucleation and growth mechanisms. We will also explore other systems with large dipole moments (e.g., propyne, dipole = 0.7 D)⁶⁵ to further test the effects of electric fields.

ACKNOWLEDGMENTS

This work was supported by the U.S. Department of Energy (DOE), Office of Science, Office of Basic Energy Sciences, Division of Chemical Sciences, Geosciences, and Biosciences. This research was performed using EMSL, a national scientific user facility sponsored by DOE's Office of Biological and Environmental Research and located at Pacific Northwest National Laboratory, which is operated by Battelle for the DOE.

DATA AVAILABILITY

The data that support the findings of this study are available from the corresponding author upon reasonable request.

REFERENCES

- 1 I. Villegas and M. J. Weaver, “Progressive cation solvation at Pt(111) model electrochemical interfaces in ultrahigh vacuum as probed by infrared spectroscopy and work-function measurements,” *Electrochim. Acta* **41**, 661 (1996).
- 2 S. Baldelli, G. Mailhot, P. Ross, Y.-R. Shen, and G. A. Somorjai, “Potential dependent orientation of acetonitrile on platinum (111) electrode surface studied by sum frequency generation,” *J. Phys. Chem. B* **105**, 654 (2001).
- 3 S. B. Waldrup and C. T. Williams, “Acetonitrile adsorption on polycrystalline platinum: An *in situ* investigation using sum frequency spectroscopy,” *J. Phys. Chem. C* **112**, 219 (2008).
- 4 G. Feng, J. Huang, B. G. Sumpter, V. Meunier, and R. Qiao, “Structure and dynamics of electrical double layers in organic electrolytes,” *Phys. Chem. Chem. Phys.* **12**, 5468 (2010).
- 5 G. H. Lane and E. Jezek, “Electrochemical studies of acetonitrile based supercapacitor electrolytes containing alkali and alkaline earth metal cations,” *Electrochim. Acta* **150**, 173 (2014).
- 6 Y. Yamada, K. Furukawa, K. Sodeyama, K. Kikuchi, M. Yaegashi, Y. Tateyama, and A. Yamada, “Unusual stability of acetonitrile-based superconcentrated electrolytes for fast-charging lithium-ion batteries,” *J. Am. Chem. Soc.* **136**, 5039 (2014).
- 7 S. V. Pavlov and S. A. Kisenko, “Effects of carbon surface topography on the electrode/electrolyte interface structure and relevance to Li-air batteries,” *Phys. Chem. Chem. Phys.* **18**, 30830 (2016).
- 8 S. Zhang, Z. Bo, H. Yang, J. Yang, L. Duan, J. Yan, and K. Cen, “Insights into the effects of solvent properties in graphene based electric double-layer capacitors with organic electrolytes,” *J. Power Sources* **334**, 162 (2016).

- ⁹I. A. Pašti, A. Marković, N. Gavrilov, and S. V. Mentus, "Adsorption of acetonitrile on platinum and its effects on oxygen reduction reaction in acidic aqueous solutions—combined theoretical and experimental study," *Electrocatalysis* **7**, 235 (2016).
- ¹⁰P. M. Solomon, K. B. Jefferts, A. A. Penzias, and R. W. Wilson, "Detection of millimeter emission lines from interstellar methyl cyanide," *Astrophys. J.* **168**, L107 (1971).
- ¹¹J. Kissel and F. R. Krueger, "The organic-component in dust from comet Halley as measured by the puma mass-spectrometer on board Vega-1," *Nature* **326**, 755 (1987).
- ¹²L. Olmi, R. Cesaroni, and C. M. Walmsley, "Ammonia and methyl cyanide in hot cores," *Astron. Astrophys.* **276**, 489 (1993).
- ¹³L. M. Lara, E. Lellouch, J. J. López-Moreno, and R. Rodrigo, "Vertical distribution of titan's atmospheric neutral constituents," *J. Geophys. Res.: Planets* **101**, 23261, <https://doi.org/doi:10.1029/96je02036> (1996).
- ¹⁴A. Marten, T. Hidayat, Y. Biraud, and R. Moreno, "New millimeter heterodyne observations of titan: Vertical distributions of nitriles HCN, HC₃N, CH₃CN, and the isotopic ratio ¹⁵N/¹⁴N in its atmosphere," *Icarus* **158**, 532 (2002).
- ¹⁵M. F. A'Hearn, M. J. S. Belton, W. A. Delamere, J. Kissel, K. P. Klaasen, L. A. McFadden, K. J. Meech, H. J. Melosh, P. H. Schultz, J. M. Sunshine, P. C. Thomas, J. Veerka, D. K. Yeomans, M. W. Baca, I. Busko, C. J. Crockett, S. M. Collins, M. Desnoyer, C. A. Eberhardy, C. M. Ernst, T. L. Farnham, L. Feaga, O. Groussin, D. Hampton, S. I. Ipatov, J.-Y. Li, D. Lindler, C. M. Lisse, N. Mastrodemos, W. M. Owen, J. E. Richardson, D. D. Wellnitz, and R. L. White, "Deep impact: Excavating comet Tempel 1," *Science* **310**, 258 (2005).
- ¹⁶N. Fray and B. Schmitt, "Sublimation of ices of astrophysical interest: A bibliographic review," *Planet Space Sci.* **57**, 2053 (2009).
- ¹⁷E. L. Barth, "Modeling survey of ices in titan's stratosphere," *Planet Space Sci.* **137**, 20 (2017).
- ¹⁸R. L. Hudson, "Preparation, identification, and low-temperature infrared spectra of two elusive crystalline nitrile ices," *Icarus* **338**, 113548 (2020).
- ¹⁹L. J. Allamandola, M. P. Bernstein, S. A. Sandford, and R. L. Walker, "Evolution of interstellar ices," *Space Sci. Rev.* **90**, 219 (1999).
- ²⁰M. H. Moore, R. F. Ferrante, W. James Moore, and R. Hudson, "Infrared spectra and optical constants of nitrile ices relevant to titan's atmosphere," *Astrophys. J., Suppl. Ser.* **191**, 96 (2010).
- ²¹R. L. Hudson, R. F. Ferrante, and M. H. Moore, "Infrared spectra and optical constants of astronomical ices: I. Amorphous and crystalline acetylene," *Icarus* **228**, 276 (2014).
- ²²R. L. Hudson, P. A. Gerakines, and M. H. Moore, "Infrared spectra and optical constants of astronomical ices: II. Ethane and ethylene," *Icarus* **243**, 148 (2014).
- ²³M. Tylinski, R. S. Smith, and B. D. Kay, "Structure and desorption kinetics of acetonitrile thin films on Pt(111) and on graphene on Pt(111)," *J. Phys. Chem. C* **124**, 2521 (2020).
- ²⁴M. Tylinski, R. S. Smith, and B. D. Kay, "Morphology of vapor-deposited acetonitrile films," *J. Phys. Chem. A* **124**, 6237 (2020).
- ²⁵E. C. Ou, P. A. Young, and P. R. Norton, "Interaction of acetonitrile with platinum (111): More properties of the η^2 (C,N) state and new species in the submonolayer," *Surf. Sci.* **277**, 123 (1992).
- ²⁶B. A. Sexton and N. R. Avery, "Coordination of acetonitrile (CH₃CN) to platinum (111): Evidence for an η^2 (C,N) species," *Surf. Sci.* **129**, 21 (1983).
- ²⁷A. Markovits and C. Minot, "Theoretical study of the acetonitrile flip-flop with the electric field orientation: Adsorption on a Pt(111) electrode surface," *Catal. Lett.* **91**, 225 (2003).
- ²⁸W. E. Putnam, D. M. McEachern, and J. E. Kilpatrick, "Entropy and related thermodynamic properties of acetonitrile (methyl cyanide)," *J. Chem. Phys.* **42**, 749 (1965).
- ²⁹M. P. Marzocchi and M. G. Migliorini, "Raman-spectra and phase transition of crystalline CH₃CN and CD₃CN," *Spectrochim. Acta, Part A* **29**, 1643 (1973).
- ³⁰M. P. Marzocchi and S. Dobos, "Infrared-spectra and crystal-structure of CH₃CN and CD₃CN. Polarization and intensity measurements," *Spectrochim. Acta, Part A* **30**, 1437 (1974).
- ³¹B. H. Torrie and B. M. Powell, "Phase-transition in solid acetonitrile," *Mol. Phys.* **75**, 613 (1992).
- ³²R. Enjalbert and J. Galy, "CH₃CN: X-ray structural investigation of a unique single crystal. $\beta \rightarrow \alpha$ phase transition and crystal structure," *Acta Crystallogr., Sect. B: Struct. Sci.* **58**, 1005 (2002).
- ³³H. Tizek, H. Grothe, and E. Knözinger, "Gas-phase deposition of acetonitrile: An attempt to understand Ostwald's step rule on a molecular basis," *Chem. Phys. Lett.* **383**, 129 (2004).
- ³⁴C. Wu and D.-S. Yang, "Ordered structures and morphology-induced phase transitions at graphite-acetonitrile interfaces," *J. Phys. Chem. C* **123**, 22390 (2019).
- ³⁵R. S. Smith, T. Zubkov, and B. D. Kay, "The effect of the incident collision energy on the phase and crystallization kinetics of vapor deposited water films," *J. Chem. Phys.* **124**, 114710 (2006).
- ³⁶T. Zubkov, R. S. Smith, T. R. Engstrom, and B. D. Kay, "Adsorption, desorption, and diffusion of nitrogen in a model nanoporous material. I. Surface limited desorption kinetics in amorphous solid water," *J. Chem. Phys.* **127**, 184707 (2007).
- ³⁷G. A. Kimmel, J. Matthesen, M. Baer, C. J. Mundy, N. G. Petrik, R. S. Smith, Z. Dohnálek, and B. D. Kay, "No confinement needed: Observation of a metastable hydrophobic wetting two-layer ice on graphene," *J. Am. Chem. Soc.* **131**, 12838 (2009).
- ³⁸R. S. Smith, J. Matthesen, and B. D. Kay, "Desorption kinetics of methanol, ethanol, and water from graphene," *J. Phys. Chem. A* **118**, 8242 (2014).
- ³⁹R. S. Smith, R. A. May, and B. D. Kay, "Desorption kinetics of Ar, Kr, Xe, N₂, O₂, CO, methane, ethane, and propane from graphene and amorphous solid water surfaces," *J. Phys. Chem. B* **120**, 1979 (2016).
- ⁴⁰A. F. Carlsson and R. J. Madix, "Intrinsic and extrinsic precursors to adsorption: Coverage and temperature dependence of Kr adsorption on Pt(111)," *J. Chem. Phys.* **114**, 5304 (2001).
- ⁴¹D. M. Murphy and T. Koop, "Review of the vapour pressures of ice and supercooled water for atmospheric applications," *Q. J. R. Meteorol. Soc.* **131**, 1539 (2005).
- ⁴²A. G. M. Ferreira and L. Q. Lobo, "The sublimation of argon, krypton, and xenon," *J. Chem. Thermodyn.* **40**, 1621 (2008).
- ⁴³W. Wagner, T. Riethmann, R. Feistel, and A. H. Harvey, "New equations for the sublimation pressure and melting pressure of H₂O ice Ih," *J. Phys. Chem. Ref. Data* **40**, 043103 (2011).
- ⁴⁴E. L. Pace and L. J. Noe, "Infrared spectra of acetonitrile and acetonitrile-d₃," *J. Chem. Phys.* **49**, 5317 (1968).
- ⁴⁵C. N. R. Rao and K. J. Rao, *Phase Transitions in Solids* (McGraw-Hill, New York, 1978).
- ⁴⁶R. H. Doremus, *Rates of Phase Transformations* (Academic Press, New York, 1985).
- ⁴⁷C. Yuan, R. S. Smith, and B. D. Kay, "Surface and bulk crystallization of amorphous solid water films: Confirmation of 'top-down' crystallization," *Surf. Sci.* **652**, 350 (2016).
- ⁴⁸C. Yuan, R. S. Smith, and B. D. Kay, "Communication: Distinguishing between bulk and interface-enhanced crystallization in nanoscale films of amorphous solid water," *J. Chem. Phys.* **146**, 031102 (2017).
- ⁴⁹R. S. Smith, C. Yuan, N. G. Petrik, G. A. Kimmel, and B. D. Kay, "Crystallization growth rates and front propagation in amorphous solid water films," *J. Chem. Phys.* **150**, 214703 (2019).
- ⁵⁰C. Bishop, A. Gujral, M. F. Toney, L. Yu, and M. D. Ediger, "Vapor-deposited glass structure determined by deposition rate-substrate temperature superposition principle," *J. Phys. Chem. Lett.* **10**, 3536 (2019).
- ⁵¹R. S. Smith, R. A. May, and B. D. Kay, "Probing toluene and ethylbenzene stable glass formation using inert gas permeation," *J. Phys. Chem. Lett.* **6**, 3639 (2015).
- ⁵²K. L. Kearns, S. F. Swallen, M. D. Ediger, T. Wu, and L. Yu, "Influence of substrate temperature on the stability of glasses prepared by vapor deposition," *J. Chem. Phys.* **127**, 154702 (2007).
- ⁵³S. F. Swallen, K. L. Kearns, M. K. Mapes, Y. S. Kim, R. J. McMahon, M. D. Ediger, T. Wu, L. Yu, and S. Satija, "Organic glasses with exceptional thermodynamic and kinetic stability," *Science* **315**, 353 (2007).
- ⁵⁴T. Ludwig, A. R. Singh, and J. K. Nørskov, "Acetonitrile transition metal interfaces from first principles," *J. Phys. Chem. Lett.* **11**, 9802 (2020).

- ⁵⁵Simple estimates assuming that the growth rates for the crystalline phase are approximately in the range from 0.1 to 10^5 ML/s suggest that more than 105 nuclei form in a typical experiment.
- ⁵⁶J. M. Esclaine, B. Monasse, E. Wey, and J. M. Haudin, "Influence of specimen thickness on isothermal crystallization kinetics. A theoretical-analysis," *Colloid Polym. Sci.* **262**, 366 (1984).
- ⁵⁷D. J. Safarik and C. B. Mullins, "Surface phase transformation kinetics: A geometrical model for thin films of nonvolatile and volatile solids," *J. Chem. Phys.* **117**, 8110 (2002).
- ⁵⁸J. R. Espinosa, C. Navarro, E. Sanz, C. Valeriani, and C. Vega, "On the time required to freeze water," *J. Chem. Phys.* **145**, 211922 (2016).
- ⁵⁹F. Wang, V. N. Richards, S. P. Shields, and W. E. Buhro, "Kinetics and mechanisms of aggregative nanocrystal growth," *Chem. Mat.* **26**, 5 (2014).
- ⁶⁰L. Delzeit, J. P. Devlin, and V. Buch, "Structural relaxation rates near the ice surface: Basis for separation of the surface and subsurface spectra," *J. Chem. Phys.* **107**, 3726 (1997).
- ⁶¹V. Buch, B. Sigurd, J. P. Devlin, U. Buck, and J. K. Kazimirski, "Solid water clusters in the size range of tens-thousands of H₂O: A combined computational/spectroscopic outlook," *Int. Rev. Phys. Chem.* **23**, 375 (2004).
- ⁶²A. Haji-Akbari and P. G. Debenedetti, "Perspective: Surface freezing in water: A nexus of experiments and simulations," *J. Chem. Phys.* **147**, 060901 (2017).
- ⁶³S. Hussain and A. Haji-Akbari, "How to quantify and avoid finite size effects in computational studies of crystal nucleation: The case of heterogeneous ice nucleation," *J. Chem. Phys.* **154**, 014108 (2021).
- ⁶⁴R. S. Smith, J. Matthiesen, J. Knox, and B. D. Kay, "Crystallization kinetics and excess free energy of H₂O and D₂O nanoscale films of amorphous solid water," *J. Phys. Chem. A* **115**, 5908 (2011).
- ⁶⁵A. F. C. Arapiraca and J. R. Mohallem, "DFT vibrationally averaged isotopic dipole moments of propane, propyne and water isotopologues," *Chem. Phys. Lett.* **609**, 123 (2014).